

A Polarized View of the Top Asymmetry

David Krohn,^{1,*} Tao Liu,^{2,†} Jessie Shelton,^{3,‡} and Lian-Tao Wang^{4,§}

¹*Department of Physics, Harvard University, Cambridge MA, 02138*

²*Department of Physics, University of California, Santa Barbara CA, 93106*

³*Department of Physics, Yale University, New Haven CT, 06511*

⁴*Department of Physics, Enrico Fermi Institute, and Kavli Institute for Cosmological Physics, University of Chicago, Chicago IL, 60637*

Recent experimental results from the CDF collaboration which study the top forward-backward asymmetry have strengthened the case that new physics is playing a role in $t\bar{t}$ production. Here we propose a set of measurements, built from the charged lepton kinematics in semileptonic and fully leptonic $t\bar{t}$ events, designed to further probe the underlying causes of this asymmetry both at the Tevatron and at the LHC. Using a set of conservative reference models we find that measurements of the charged lepton asymmetry, top polarization, and $t\bar{t}$ spin correlation can establish the existence of new physics and distinguish between competing models both at the Tevatron and the LHC. At the Tevatron, discrimination between models is possible at the 3σ level. At the LHC, we demonstrate that a top forward-backward asymmetry can be established at $\gtrsim 3\sigma$ in the first $\sim 5 \text{ fb}^{-1}$ of data, and show how competing explanations can be further disentangled.

I. INTRODUCTION

Roughly three years ago both CDF and D0 reported anomalously large top forward-backward asymmetries (AFB) [1]. Since that time analyses have improved and integrated luminosities have increased such that the latest semileptonic results [2] from CDF report a 3.4σ discrepancy with the Standard Model (SM) prediction [3, 4] in the high $m_{t\bar{t}}$ region, while in the fully leptonic¹ channel recent measurements [5] display a 2.6σ deviation in the same direction.

During this time the theory community has dedicated much effort to model building aimed at explaining these excesses [6]. The good agreement of the top pair production cross-section with SM predictions drives most models to generate the asymmetry from interference between new physics and the standard model, leading to the introduction of either a flavor-nonuniversal s -channel colored vector boson or a t -channel color singlet with nontrivial flavor structure.

If physics beyond the Standard Model (BSM) is really responsible for the top asymmetry then it would be desirable to probe its particle content directly by producing any new states on-shell and then measuring their masses and couplings. Depending on the model, such searches may proceed in $t\bar{t}$ resonances or top-light jet resonances, and interesting signals may be discovered shortly. However, excesses in the *nonresonant* $t\bar{t}$ cross-section alone allow for observations of departures from the SM [7]. Here we establish that a BSM leptonic charge asymmetry can also be seen in nonresonant $t\bar{t}$ events at the 7 TeV LHC.

By virtue of the fact that the BSM states must have couplings strong enough to impact the measurement of AFB in the low to intermediate range of $m_{t\bar{t}}$, we can confidently measure some essential properties of relevant BSM states in a fairly model-independent way. Chief among these is the chiral nature of their couplings to the top, and the correlation between top polarizations in the final state². We further study the asymmetry with leptonic variables; together with measurements of spin correlations and polarization, models for the top asymmetry can be well tested within the 7 TeV run.

Measuring the chiral nature of the top's coupling in the region where we measure AFB would be useful because this coupling is vector-like at tree level in the SM, so any deviation from this, as is required in e.g. models with an s -channel color vector octet, would indicate the presence of new physics. Moreover, the strong constraints on b quark couplings from precision flavor observables leads many models for AFB to couple only to right-handed tops, predicting large and distinct polarization signals. Any confirmation of a non-vector-like coupling, especially one which is dominantly right-handed, would strengthen the case for new physics. Furthermore, the correlation between the top and anti-top polarizations can be used to distinguish between different production mechanisms, particularly at the LHC, where BSM contributions to the top pair production cross-section are expected to be large.

Fortunately, as the top decays before hadronization effects can wash out its polarization information, many useful spin observables can be constructed in $t\bar{t}$ events. It has been known for more than two decades that the differential distributions of top decay products serve as an excellent probe of new physics [13], with many applications to the study of $t\bar{t}$ resonances [14], and, more

* dkrohn@physics.harvard.edu

† taoliu@physics.ucsb.edu

‡ j.shelton@yale.edu

§ liantaow@uchicago.edu

¹ Here and throughout this paper we will use “leptonic” to refer only to electrons and muons.

² For recent proposals focusing on other observables, see Refs [8–12].

recently, to distinguishing potential explanations of the anomalous top AFB [15].

The main contribution of this article is the study of the power of various leptonic observables for determining the existence of an enhanced top forward-backward asymmetry and discriminating amongst competing explanations for it, using a set of relevant models and (for the LHC) a realistic top-reconstruction algorithm. We will employ a set of four phenomenological reference models to inject signals characteristic of the two basic classes of models constructed to explain the forward-backward asymmetry: (1) models with an s -channel vector boson are represented by three reference axigluon models with fully axial, left-handed, and right-handed couplings, while (2) t -channel vector boson models are represented by a reference W' . Full details of our benchmarks can be found in App. B, but it is important to note that the particular models at hand (i.e. the chosen masses and couplings) are not essential to our conclusions - other s - and t -channel models constructed to yield a similar asymmetry would yield lead us to similar conclusions.

We first consider the prospects at the Tevatron in section Sec. II, examining the potential impact of leptonic observables with current and projected luminosities at the Tevatron. We emphasize that leptonic observables access novel information beyond that contained in the distributions of the parent tops, and compare the utility of measuring polarization directly versus indirectly, through lepton charge asymmetries [3, 15]. In Sec. III we will build upon prior works [15] and present a detailed set of cuts and observables which allow for useful probes of relevant BSM physics within the first $1 - 5 \text{ fb}^{-1}$ of 7 TeV LHC data. In particular, we will see that a leptonic charge asymmetry in dileptonic $t\bar{t}$ events can be established at $\geq 3\sigma$ in 5fb^{-1} for all of our BSM reference models. Sec. IV contains our conclusions. Finally, in App. A we give an overview of our top reconstruction procedure, App. B discusses our benchmark models, and App. C contains many tabulated results.

II. TEVATRON ANALYSIS

As was mentioned in Sec. I, the polarization of the top is reflected in the kinematic distributions of its daughters, as the top decays before hadronization effects can wash away this information. Thus top polarization \mathcal{P}_n along a chosen axis \hat{n} can be measured by the angular distribution of the top decay products with respect to that axis, measured in the top rest frame [16]:

$$\frac{1}{\Gamma} \frac{d\Gamma}{d \cos \theta_{i,n}} = \frac{1}{2} (1 + \mathcal{P}_n \kappa_i \cos \theta_{i,n}) \quad (1)$$

where $\mathcal{P}_n = \pm 1$ for tops completely polarized (anti-) parallel with the chosen axis, κ_i is the *spin analyzing power* of decay product i , and θ_i is the direction of each daughter with respect to the chosen axis, as measured in the rest frame of the top. For the b we have $\kappa = -0.4$, while

for the neutrino $\kappa = -0.3$, and the charged lepton has $\kappa = 1.0$. Thus, of all the particles coming from the decay of the top the charged lepton is most sensitive to the top's polarization.

The high sensitivity of the charged lepton is convenient, because of all the top decay products it is the easiest to identify and measure. The purpose of this section is to point out that simple variables constructed from the leptons in semileptonic and dileptonic $t\bar{t}$ events have hitherto untapped power to distinguish between competing explanations of the observed asymmetry even at the Tevatron, and have the potential to significantly strengthen the case for new physics beyond the standard model. Models which attempt to explain the observed top asymmetry typically predict heavy new states with nontrivial chiral structure. This translates into a potentially large net polarization of tops as well as a departure from SM spin correlations, and therefore potentially large signals in the lepton distributions which are capable of distinguishing between different models [15].

For a given choice of axis \hat{n} , the net polarization of the top sample along that axis can be extracted as

$$\mathcal{P}_n = \frac{N(\cos \theta_{\ell,n} > 0) - N(\cos \theta_{\ell,n} < 0)}{N(\cos \theta_{\ell,n} > 0) + N(\cos \theta_{\ell,n} < 0)}. \quad (2)$$

Three commonly considered polarization bases are (1) \mathcal{P}_h , the helicity basis, where \hat{n} is given by the direction of the parent top's momentum in the CM frame; (2) \mathcal{P}_b , the beam basis, where \hat{n} is given by the direction of the beam; and (3) $\mathcal{P}_{\text{off-d}}$, the off-diagonal axis [17], which maximizes SM spin correlations and interpolates between the previous two. The SM predicts a small net polarization arising from electroweak corrections to top pair production, which we neglect³. After imposing selection cuts [2, 5] as discussed below, however, SM tops will in general show a nonzero polarization. In Table I we display these values as well as predictions for our reference models in the helicity basis. Results for the beam and off-diagonal bases are shown in Table XIV and Table XV in the Appendix. The helicity basis gives better separation between BSM models and the SM at the Tevatron than either the beam basis or the off-diagonal basis. This is not surprising: the helicity basis becomes optimal when the top mass is small compared to its energy, while the beam basis is effective when the top is traveling with a small velocity, precisely where contributions from BSM physics are smallest relative to the standard model. Top polarization from new physics will be larger at higher invariant mass where the helicity basis is better suited. The off-diagonal basis, which interpolates between the beam basis and the helicity basis, is intermediate in sensitivity.

³ The corrections obtained from SM EW processes will at most shift our observables by a small linear amount and will not have any qualitative effect on our conclusions.

	Semileptonic		Dileptonic	
	sel. cuts	$m_{t\bar{t}} > 450$ GeV	sel. cuts	$m_{t\bar{t}} > 450$ GeV
SM	4 % (3 %)	7 % (5 %)	4 % (6.5 %)	6 % (10 %)
G_A	5 %	7 %	5 %	7 %
G_L	2 %	-1 %	1 %	-1 %
G_R	8 %	12 %	8 %	12 %
W'	15 %	22 %	14 %	21 %

TABLE I. Net polarization \mathcal{P}_h in the helicity basis at the Tevatron. We note that in the SM, at tree-level, these asymmetries are all zero. In parentheses are 1σ statistical errors uncertainties on an asymmetry measurement centered about the predicted SM value assuming 5.3fb^{-1} (semileptonic) or 5.1fb^{-1} (dileptonic). Note that the effects of the differing semileptonic and dileptonic selection cuts are small.

The lepton polarization angle $\cos\theta_\ell$ has the nice feature that it is completely uncorrelated with the kinematics of the parent tops as it is measured in the top rest frame. However, reconstructing this frame is non-trivial and can be difficult. It is possible to define other variables which use the same underlying information, but may prove more flexible. One especially interesting variable is the *leptonic charge asymmetry* [3, 15]

$$\mathcal{A}_{FB}^\ell = \frac{N(q\ell y_\ell > 0) - N(q\ell y_\ell < 0)}{N(q\ell y_\ell > 0) + N(q\ell y_\ell < 0)} \quad (3)$$

in semileptonic events. The charged lepton rapidity (in either the lab or the CM frame) depends on the velocity β_t and CM frame production angle $\cos\theta_t$ of the semileptonic top as well as on $\cos\theta_\ell$, but is independent of the lepton energy in the top rest frame (as the lepton is effectively massless, and so the energy only changes the magnitude of its four-vector). Thus the lepton asymmetry of Eq. (3) is an alternate measure of the lepton polarization: it contains additional information about the top production mechanism, beyond the information in the top AFB. We illustrate the relationship between top and lepton rapidities in Fig. 1. For dileptonic tops, one can define the *dileptonic charge asymmetry*,

$$\mathcal{A}_{FB}^{\Delta\ell} = \frac{N((y_{\ell^+} - y_{\ell^-}) > 0) - N((y_{\ell^+} - y_{\ell^-}) < 0)}{N((y_{\ell^+} - y_{\ell^-}) > 0) + N((y_{\ell^+} - y_{\ell^-}) < 0)} \quad (4)$$

which is frame-independent. As can be seen in Fig. 1, the dependence of lepton rapidity on parent top polarization is enhanced in the forward regions. Therefore a new source of right-handed tops which preferentially populates high rapidity regions will lead to a significant enhancement of forward leptons. As central lepton acceptance at the Tevatron extends only to $|\eta| < 1.1$, this can lead to marked acceptance differences between BSM and SM tops, as well as differences between the BSM models themselves. In particular, acceptances need to be understood separately for t -channel right-handed models and s -channel axially-coupled models (see also [10]).

While the correlation between the lepton asymmetries \mathcal{A}_{FB}^ℓ , $\mathcal{A}_{FB}^{\Delta\ell}$ and the top forward-backward asymmetry $\mathcal{A}_{FB}^{t\bar{t}}$ is less direct than a direct measurement of

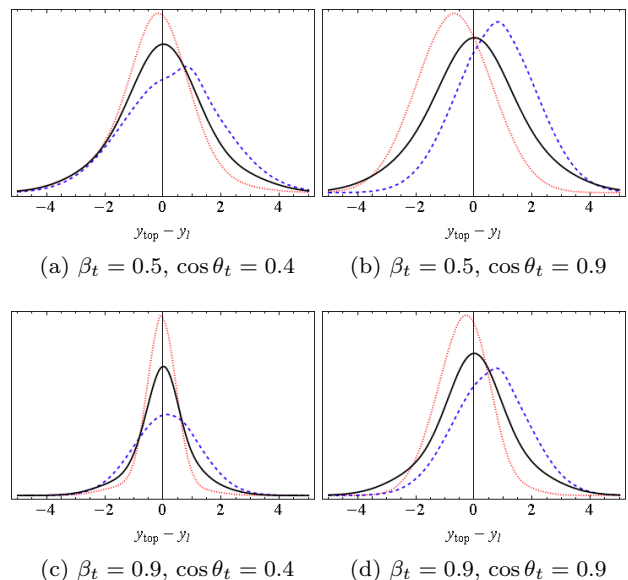


FIG. 1. Distributions of the rapidity difference $y_{top} - y_\ell$ for right-handed (red, dotted), left-handed (blue, dashed) and unpolarized (black, solid) tops, for fixed top kinematics as determined by the top boost β_t and CM frame production angle $\cos\theta_t$.

the top polarization through the top rest frame variable of Eq. (2), the lepton asymmetry does not require reconstruction of rest frames and can therefore provide a cleaner probe of the system. Moreover, as the lepton is not colored, a measurement of the lepton asymmetry allows for easier comparison to predictions from NLO QCD⁴. In the absence of any polarization, a given top asymmetry $\mathcal{A}_{FB}^{t\bar{t}}$ will produce a mildly reduced \mathcal{A}_{FB}^ℓ . Left-handed tops, however, will yield a much reduced \mathcal{A}_{FB}^ℓ , while for right-handed tops the leptonic asymmetry is comparable to or greater than the parent top asymmetry. If the tops are sufficiently forward that finite lepton acceptance becomes relevant (i.e., if the top is sufficiently forward then events which would contribute to the asymmetry will not pass selection cuts - we will see this for the W' model) then this conclusion will not hold.

In the following subsections we consider semileptonic and dileptonic tops at the Tevatron in more detail, focusing on lepton charge asymmetries. All results are simulated using the full $2 \rightarrow 6$ matrix elements of $t\bar{t}$ production as computed in Madgraph [18].

A. Semileptonic Tops

For semileptonic tops, we impose selection cuts after [2], requiring: a charged lepton with $|\eta| < 1.0$ and $p_{T\ell} > 20$ GeV; at least four jets with $p_{Tj} > 40$ GeV and $|\eta| < 2.0$; and missing energy $\cancel{E}_T > 20$ GeV. Further, at least one jet must be b -tagged, which means the tagged jet

⁴ Thanks to K. Melnikov for emphasizing this point.

frame and mass range	$t\bar{t}$ asymmetry	Lepton asymmetry	stat. sig. (5.3 fb ⁻¹)
G_A lab, sel. cuts	9 %	4 %	1.1
lab, $m_{t\bar{t}} > 450$ GeV	17 %	9 %	1.9
CM, sel. cuts	12 %	6 %	1.7
CM, $m_{t\bar{t}} > 450$ GeV	19 %	12 %	2.4
G_L lab, sel. cuts	7 %	-3 %	0.9
lab, $m_{t\bar{t}} > 450$ GeV	14 %	-1 %	0.2
CM, sel. cuts	13 %	-4 %	1.4
CM, $m_{t\bar{t}} > 450$ GeV	20 %	-3 %	0.6
G_R lab, sel. cuts	9 %	12 %	3.9
lab, $m_{t\bar{t}} > 450$ GeV	14 %	18 %	5.0
CM, sel. cuts	9 %	16 %	3.5
CM, $m_{t\bar{t}} > 450$ GeV	15 %	22 %	4.4
W' lab, sel. cuts	15 %	13 %	3.9
lab, $m_{t\bar{t}} > 450$ GeV	26 %	22 %	4.9
CM, sel. cuts	20 %	16 %	4.4
CM, $m_{t\bar{t}} > 450$ GeV	31 %	26 %	5.3

TABLE II. BSM contributions to the parton level $t\bar{t}$ and leptonic asymmetries after imposing CDF semileptonic acceptance cuts. Lepton asymmetries computed using both the lab and CM frame lepton rapidities are shown. We note that in the SM, at tree-level, these asymmetries are all zero. Statistical significances of the leptonic asymmetries are based on the number of events observed in [2].

must be central, $|\eta_b| < 1.0$. After these cuts, non-top background is less than $\mathcal{O}(20\%)$ of remaining events; we neglect it here. In what follows we will present results with statistical errors derived from the published number of events measured at CDF.

In Table II, we compare the leptonic charge asymmetry to the parent top asymmetry in our reference models. The contribution to the asymmetries from LO SM $t\bar{t}$ is zero for all asymmetries even after selection cuts. We quote statistical significance of the leptonic asymmetries based on the number of events observed in 5.3 fb^{-1} . By the end of the Tevatron's run, twice this amount of data will be available (for each experiment); as the statistical uncertainties scale approximately as $1/\sqrt{N}$, the maximum statistical reach of the Tevatron is larger by nearly a factor of two (after combining the data of both experiments).

Unsurprisingly, the lepton asymmetry in the CM frame is a more sensitive probe than the lab frame lepton asymmetry. However, we emphasize that even the simple lab frame variable, which requires no leptonic top reconstruction and is consequently free of many systematics, can (1) help to establish the existence of an asymmetry inconsistent with SM predictions, and (2) begin to distinguish between competing models for the asymmetry.⁵

⁵ Defining the visible mass as the invariant mass of the lepton plus the 4 hard jets identified as the visible $t\bar{t}$ decay products, enables efficient isolation of high \sqrt{s} events without reconstructing the leptonic top. Using a high *visible* mass bin $m_{vis} > 375$ GeV yields a comparable enhancement to using a high total mass bin $m_{t\bar{t}} > 450$.

The relationship between the lepton asymmetry and the parent top asymmetry is a distinctive feature of the models: for the axigluon models, which have similar top kinematics, the asymmetry is slightly reduced due to kinematics for G_A , dramatically reduced for G_L , and enhanced for G_R . The W' , although similar to the G_R in yielding a higher proportion of right-handed tops, shows proportionally less of an enhancement of the lepton asymmetry; this is because the W' produces tops which are more forward, where limited y acceptance for leptons causes events to fail acceptance cuts.

In Table II it is evident that the W' model can be distinguished from both the SM and the other reference models at $\gtrsim 3\sigma$. Our reference models G_R and W' predict similar central values for the lepton asymmetries but larger top asymmetries for the W' model. With the cuts in [2], the CM frame top asymmetries differ by nearly 3σ for G_R and W' . The full anticipated Tevatron data set allows a lepton asymmetry to be established at more than 3σ for all models except the G_L . Meanwhile, the G_L model has a very distinctive signal of a lepton asymmetry near zero, which in the presence of a significant top asymmetry is distinguishing. Moreover, the G_A and W' models can be discriminated at more than 3σ . One might worry that this distinction is artificial, as the G_A model is chosen to underpredict the top asymmetry while the W' model is not. However, for comparison purposes we have also examined an axial axigluon parameter point G'_A with larger couplings (but the same mass and width) than the model displayed in Table II. This model overpredicts the Tevatron $t\bar{t}$ cross-section but has the same central values for the CM frame top asymmetries as the W' . In this modified G'_A model, the lepton asymmetries are nearly 3σ smaller than in the W' model. Thus with the full anticipated data set the Tevatron has the potential to discriminate between these explanations at $\gtrsim 3\sigma$ by exploiting the characteristic differences in the lepton asymmetries relative to the asymmetry of the parent top.

B. Dileptonic tops

While dileptonic tops at the Tevatron are limited by both statistical and kinematic reach, results from this channel are interesting especially in combination with the semileptonic channel. For dileptonic tops, we impose selection cuts after [5]. Specifically, we require two opposite sign leptons, with $p_T > 20$ GeV and $|\eta| < 1.1$ for electrons, $|\eta| < 0.6$ for muons; at least two jets satisfying $p_T > 15$ GeV and $|\eta| < 2.5$; and large missing energy, $\cancel{E}_T > 50$ GeV. In addition a cut is placed on the scalar sum of the transverse energy of the leptons, missing energy, and jets, $H_T \equiv \cancel{E}_T + p_{T\ell_i} + p_{Tj_i} > 200$ GeV. After these cuts, the dominant backgrounds are fakes, followed by Drell-Yan production of lepton pairs; signal makes up 70% of the events passing the cuts.

At the Tevatron, the most useful variables in dileptonic tops are again (1) the polarization angle $\cos\theta_\ell$

TABLE III. New physics contributions to the dileptonic asymmetry. Results are shown for reference models after imposing CDF dileptonic acceptance cuts as in [5]. Statistical significances are based on the number of signal events observed in [5].

mass range	asymmetry (5.1 fb ⁻¹)	stat. sig.
G_A sel. cuts	8 %	1.2
$m_{t\bar{t}} > 450$ GeV	14 %	1.4
G_L sel. cuts	-4 %	0.5
$m_{t\bar{t}} > 450$ GeV	1 %	0
G_R sel. cuts	15 %	2.4
$m_{t\bar{t}} > 450$ GeV	20 %	2.1
W' sel. cuts	15 %	2.3
$m_{t\bar{t}} > 450$ GeV	24 %	2.6

(see Table I) and (2) the dileptonic charge asymmetry of Eq. (4). In Table III, we show the dileptonic charge asymmetry in our reference models, and quote statistical significances based on the number of events observed in 5.1 fb⁻¹. While the smaller branching ratios into the dileptonic channel limit the statistical reach compared to the semileptonic channel, with the full data set a leptonic asymmetry can be established at more than 3σ for the right-handed models, G_R and W' . Other dileptonic variables, such as those we will consider for the LHC in the next section, are less sensitive at the Tevatron.

III. LHC STUDIES

We now turn our attention to the LHC to see what light it can shed upon any new physics effects contributing to the top asymmetry measured at the Tevatron.

At first sight, measuring a charge asymmetry might seem impossible: the LHC, unlike the Tevatron, collides identical particles (i.e. pp instead of $p\bar{p}$) and it is unclear how an asymmetry might be observed in this setup. However, while the initial state particles are symmetric at the LHC, the quark and anti-quark parton distributions within them are not, with valence quarks dominating over sea quarks at high x . Thus, if the $t\bar{t}$ system is left-moving then it is more likely to come from a left-moving quark and a right-moving anti-quark than the other way around, and vice-versa [4, 8, 11].

We will make use of this correlation between the boost of the $t\bar{t}$ system and the partonic forward direction and adapt the observables defined in the previous section to a pp collider. We will first show that, if the Tevatron excess is due to contribution from new physics, it can be confirmed at least at 3σ level with the first 5 fb⁻¹ of LHC data. At the same time, purely leptonic observables with only minimal dependence on event reconstruction are effective in probing the new physics. We will also find that measurements of the top quark polarization and $t\bar{t}$ spin correlations can serve as powerful tools to distinguish dif-

TABLE IV. The cross section, in pb, for leptonically decaying di-top events at a 7 TeV LHC.

	G_A	G_L	G_R	W'	SM
Selection cuts	1.3	1.4	1.4	2.1	1.3
$m_{t\bar{t}} > 450$ GeV	0.7	0.7	0.7	1.3	0.6
$ y(t) + y(\bar{t}) > 2$	0.2	0.2	0.2	0.3	0.2

TABLE V. The top forward-backward asymmetry ($A^{t\bar{t}}$) at a 7 TeV LHC, and in parenthesis the 1σ statistical uncertainties, (i.e. $1/\sqrt{N}$) assuming 5 fb⁻¹ of data.

	$G_A(\%)$	$G_L(\%)$	$G_R(\%)$	$W'(\%)$	SM($\%$)
Selection cuts	3	2	4	14	1 (± 1.2)
$m_{t\bar{t}} > 450$ GeV	5	3	6	20	0 (± 1.7)
$ y(t) + y(\bar{t}) > 2$	8	5	12	36	1 (± 3.2)

ferent new physics scenarios.

We first describe the details of our simulation and our choices of selection cuts. As in the previous section, parton-level samples are again generated using the full $2 \rightarrow 6$ processes in Madgraph [18]. However, here we will present results more sensitive to top reconstruction and thus a more accurate simulation is warranted. Therefore, we further shower the parton-level events in Pythia [19], cluster the visible particles into 0.1×0.1 calorimeter cells between $-5 < \eta < 5$, and form $R = 0.7$ anti- k_T [20] jets using Fastjet [21]⁶. The jets and leptons in our reconstructed events are then passed through a realistic top reconstruction algorithm (see App. A) which is used to calculate our observables.

To select dileptonic tops, we employ a set of selection cuts adapted from Ref. [22]. These cuts require two hard ($p_{T\ell} > 20$ GeV), central leptons ($|y_\ell| < 2.5$) with an invariant mass outside the Z window ($76 \text{ GeV} < m_{\ell+\ell-} < 106 \text{ GeV}$), two hard, central jets ($p_{Tj} > 30$ GeV, $|y_j| < 2.5$), and missing energy ($\cancel{E}_T > 25$ GeV). These cuts reduce the backgrounds to di-top production to the $\mathcal{O}(20\%)$ level, and so in what follows we will ignore them.

To further isolate the effects of new physics we place a cut on the reconstructed $t\bar{t}$ invariant mass

$$m_{t\bar{t}} > 450 \text{ GeV.} \quad (5)$$

At large $m_{t\bar{t}}$, the behavior of the observables considered later in this section depends further on the details of the underlying new physics model. For example, the axigluon-like models typically have a broad resonance centered between 1 – 2 TeV, and the resulting observables in the regime of $m_{t\bar{t}} > 1$ TeV are sensitive to the

⁶ For comparison, parton level results are tabulated in Appendix C.

precise location and width of the resonance. Such dependence can provide valuable information. Instead of pursuing this further, we focus instead on the more universal nonresonant portion of the $t\bar{t}$ spectrum, imposing an *upper bound* $m_{t\bar{t}} < 1.5$ TeV. This represents a conservative approach.

Finally, since the process $gg \rightarrow t\bar{t}$ has a symmetric initial state it cannot contribute to the asymmetry in $t\bar{t}$ production measured at the Tevatron, and thus constitutes a background to the $q\bar{q} \rightarrow t\bar{t}$ process we wish to observe. Now, as the gluon PDFs fall more rapidly at large x than quark PDFs, the gluon-initiated contribution to top pair production tends to be more central than the $q\bar{q}$ -initiated contribution. To suppress the symmetric background from $gg \rightarrow t\bar{t}$, we employ a cut

$$|y_t + y_{\bar{t}}| > 2, \quad (6)$$

which restricts $t\bar{t}$ production to the relatively forward region. The cut is chosen so that the contributions to $t\bar{t}$ production from gg and $q\bar{q}$ are roughly comparable in this regime. In addition, it also increases the correlation between the boost of the $t\bar{t}$ system and the direction of the incoming quark.

The total $t\bar{t}$ production cross sections for the reference models, including both the Standard Model and new physics contributions, after imposing these cuts successively are shown in Table IV. For comparison, the Standard Model production rates are also displayed. Assuming 5 fb^{-1} of data, we estimate the $1\sigma = 1/\sqrt{N}$ fractional statistical uncertainties (shown in parenthesis).

A. Top forward backward asymmetry $\mathcal{A}^{t\bar{t}}$

One can generalize the forward-backward asymmetry $\mathcal{A}^{t\bar{t}}$ to a symmetric (pp) collider⁷ by defining it as

$$\mathcal{A}^{t\bar{t}} = \frac{N(0 < \hat{\theta}_t < \pi/2) - N(\pi/2 < \hat{\theta}_t < \pi)}{N(0 < \hat{\theta}_t < \pi/2) + N(\pi/2 < \hat{\theta}_t < \pi)}, \quad (7)$$

where $\hat{\theta}_t$ is the production angle of the top quark in the $t\bar{t}$ center of mass frame with respect to the direction of the boost of the $t\bar{t}$ system. Note that the 1σ estimated in Table V can also be used as a measure of the deviation of an $\mathcal{A}^{t\bar{t}}$ measurement from the Standard Model prediction which is approximately zero. Based on the procedure described in Appendix A, we reconstruct the kinematics of the top quark and calculate the $\mathcal{A}^{t\bar{t}}$ in various models. The results are shown in Table V. It can be seen from Table V that in all but one of the conservative reference models, the new physics contribution to the $\mathcal{A}^{t\bar{t}}$ can be identified at the LHC at the level of $\gtrsim 3\sigma$. The only exception is the G_L model, whose contribution to

$\mathcal{A}^{t\bar{t}}$ can only be detected at a level just below 2σ . This is mainly due to the bias introduced by our selection cut. As discussed in the previous section, the direction of the lepton is (anti)correlated with the (left)right polarized tops. Therefore, the boost of higher energy tops satisfying Eq. 5 will necessarily result in harder (softer) leptons. Combining with the lepton p_T cut, this effect leads to the relative enhancement of the signal from the G_R model relative to the G_L model. We will observe the same bias in other observables discussed later in this section.

Note that although the rapidity cut in Eq. 6 does help to enhance the observed asymmetry, the asymmetry is already visible after imposing the cut on $m_{t\bar{t}}$. Omitting the stringent cut on $t\bar{t}$ rapidity will certainly enhance the signal statistics, as shown in Table IV. As we will see in the rest of this section, the relative merit of including the rapidity cut depends on the specific observable under discussion. Therefore, we will base our conclusions only on the most effective set of cuts.

From Table V, there are also observable difference between various new physics scenarios. In particular, the W' gives the largest asymmetry. This is consistent with the pattern which is already noticeable for $\mathcal{A}^{t\bar{t}}$ at the Tevatron, but it is much more striking at the LHC. This relative enhancement is due to the fact that in the W' model the new physics scale is much lower than in axi-gluon models, so the increase in center-of-mass energy greatly increases the fraction of time spent near the Rutherford singularity. The analogous situation for an axigluon would be probing near the pole mass, but to present a conservative model-independent estimate we have removed this singularity (indeed, were we to have included and used a low mass, our axigluon results could have shown similarly large effects). We will also observe the same pattern in the other observables discussed later in this section.

Within the axigluon models, we expect to observe a smaller $\mathcal{A}^{t\bar{t}}$. Even in this case, we can gather early indications of whether the underlying new physics model is of the G_A type. In the following, we will turn to additional observables to help both in enhancing the signal significance, and distinguishing among different axigluon models.

B. (Nearly) Purely Leptonic Observables

The first set of observables we will consider are those which involve only leptons, and thus have only a minimal dependence on event reconstruction⁸. We consider the generalization of the dilepton charge asymmetry to a

⁷ Related observables have been considered before in [4, 8, 11]

⁸ Cuts like Eq. (5) require reconstruction of the $t\bar{t}$ system, and thus can affect the distribution of even purely leptonic observables by biasing which events are selected.

TABLE VI. The forward-central lepton asymmetry \mathcal{A}_{FC}^ℓ at the 7 TeV LHC, and in parenthesis the 1σ statistical uncertainties, (i.e. $1/\sqrt{N}$) assuming 5 fb^{-1} of data.

	$G_A(\%)$	$G_L(\%)$	$G_R(\%)$	$W'(\%)$	SM($\%$)
Selection cuts	2	0	5	13	0 (± 1.2)
$m_{t\bar{t}} > 450 \text{ GeV}$	4	2	7	19	-1 (± 1.7)
$ y(t) + y(\bar{t}) > 2$	7	2	14	35	1 (± 3.2)

symmetric collider:

$$\mathcal{A}_{FC}^\ell = \frac{N(|y_{\ell+}| > |y_{\ell-}|) - N(|y_{\ell-}| > |y_{\ell+}|)}{N(|y_{\ell+}| > |y_{\ell-}|) + N(|y_{\ell-}| > |y_{\ell+}|)}, \quad (8)$$

measuring a *forward-central* leptonic charge asymmetry. We present the measurement of this observable in Table VI. As at the Tevatron, the leptonic charge asymmetry is a powerful probe of the existence of a BSM asymmetry. As can be seen from Table VI, it allows $\gtrsim 3\sigma$ discrimination of all models except the G_L from the SM with order a few inverse femtobarn of data, and much sooner in the case of the W' . Moreover, the G_R model becomes distinguishable from the others. Thus the dileptonic charge asymmetry can establish the existence of a BSM asymmetry in $t\bar{t}$ events in typical axigluon or t -channel vector boson models in the expected 7 TeV run.

To further strengthen the case for new physics and distinguish between competing explanations of an asymmetry, we consider several other leptonic variables. The combination of these variables provides a diagnostic suite of measurements which, taken together, can distinguish between different models for the top AFB.

One useful variable is the asymmetry in the azimuthal angle between the two leptons, $\Delta\phi$, which is π when the two leptons are back to back and zero when they are aligned in the transverse plane. In Eq. (9) we construct an asymmetry with this variable

$$\mathcal{A}_{\Delta\phi}^{\ell\ell} = \frac{N(\cos \Delta\phi_{\ell\ell} > 0) - N(\cos \Delta\phi_{\ell\ell} < 0)}{N(\cos \Delta\phi_{\ell\ell} > 0) + N(\cos \Delta\phi_{\ell\ell} < 0)}. \quad (9)$$

measuring how often the two leptons are on opposite sides of the transverse plane (contributing to $\mathcal{A}_{\Delta\phi}^{\ell\ell} < 0$) vs. how often they are on the same side ($\mathcal{A}_{\Delta\phi}^{\ell\ell} > 0$). Unlike the leptonic asymmetry constructed in Eq. (8), there is a kinematic reason for $\mathcal{A}_{\Delta\phi}^{\ell\ell}$ to be biased to negative values. However, as one can see in Table VII, the difference between the various $\mathcal{A}_{\Delta\phi}^{\ell\ell}$ provides a useful discriminant. In particular, it helps in distinguishing the signal of the W' and G_R models from the Standard Model. We note that this variable is not as sensitive as the others considered, and is not useful at the Tevatron where new physics is probed at lower energies and with smaller statistics.

TABLE VII. The azimuthal angle asymmetry $\mathcal{A}_{\Delta\phi}^\ell$ at a 7 TeV LHC, and in parenthesis the 1σ statistical uncertainties, (i.e. $1/\sqrt{N}$) assuming 5 fb^{-1} of data

	$G_A(\%)$	$G_L(\%)$	$G_R(\%)$	$W'(\%)$	SM($\%$)
Selection cuts	-26	-26	-28	-43	-24 (± 1.2)
$m_{t\bar{t}} > 450 \text{ GeV}$	-47	-47	-50	-62	-45 (± 1.7)
$ y(t) + y(\bar{t}) > 2$	-45	-44	-49	-56	-45 (± 3.2)

TABLE VIII. Net polarization \mathcal{P}_b in the beam basis at a 7 TeV LHC, and in parenthesis the 1σ statistical uncertainties, (i.e. $1/\sqrt{N}$) assuming 5 fb^{-1} of data

	$G_A(\%)$	$G_L(\%)$	$G_R(\%)$	$W'(\%)$	SM($\%$)
Selection cuts	4	-1	5	9	2 (± 1.2)
$m_{t\bar{t}} > 450 \text{ GeV}$	1	-4	4	11	0 (± 1.7)
$ y(t) + y(\bar{t}) > 2$	2	-5	7	15	1 (± 3.2)

C. Top Polarization

As one might expect, fully reconstructed observables are even more powerful than those which use only the leptons. Next we explore top polarization measurements, which again require reconstruction of the top rest frame. For simplicity we consider two choices of polarization axis: (1) the beam axis, which we now define relative to the boost of the $t\bar{t}$ system,

$$\hat{n}_{\text{beam}} = \begin{cases} +\hat{z} & \text{if } y_t + y_{\bar{t}} > 0 \\ -\hat{z} & \text{if } y_t + y_{\bar{t}} < 0 \end{cases} \quad (10)$$

and (2) the helicity axis, again defined as the top direction of motion in the $t\bar{t}$ center of mass frame. The asymmetry in $\cos\theta_\ell$ which measures the net polarization does not need to be redefined for the LHC, so we have once again

$$\mathcal{P}_n = \frac{N(\cos\theta_{\ell,n} > 0) - N(\cos\theta_{\ell,n} < 0)}{N(\cos\theta_{\ell,n} > 0) + N(\cos\theta_{\ell,n} < 0)}. \quad (11)$$

Results are tabulated for the beam axis in Table VIII and for the helicity axis in Table IX.

Polarization measurements are particularly useful for distinguishing among the various axigluon models, which differ from each other chiefly in the chiralities of their

TABLE IX. Net polarization \mathcal{P}_h in the helicity basis at a 7 TeV LHC, and in parenthesis the 1σ statistical uncertainties, (i.e. $1/\sqrt{N}$) assuming 5 fb^{-1} of data

	$G_A(\%)$	$G_L(\%)$	$G_R(\%)$	$W'(\%)$	SM($\%$)
Selection cuts	1	-1	4	18	1 (± 1.2)
$m_{t\bar{t}} > 450 \text{ GeV}$	2	-2	6	26	0 (± 1.7)
$ y(t) + y(\bar{t}) > 2$	0	-4	3	19	-2 (± 3.2)

TABLE X. Spin correlation $\mathcal{A}_{c_1 c_2}^\ell$ in the beam basis at a 7 TeV LHC, and in parenthesis the 1σ statistical uncertainties, (i.e. $1/\sqrt{N}$) assuming 5 fb^{-1} of data

	$G_A(\%)$	$G_L(\%)$	$G_R(\%)$	$W'(\%)$	SM(%)
Selection cuts	-2	-2	-2	-9	-1 (± 1.2)
$m_{t\bar{t}} > 450 \text{ GeV}$	-3	-3	-2	-11	0 (± 1.7)
$ y(t) + y(\bar{t}) > 2$	-5	-4	-1	-11	-1 (± 3.2)

TABLE XI. Spin correlation $\mathcal{A}_{c_1 c_2}^\ell$ in the helicity basis at a 7 TeV LHC, and in parenthesis the 1σ statistical uncertainties, (i.e. $1/\sqrt{N}$) assuming 5 fb^{-1} of data

	$G_A(\%)$	$G_L(\%)$	$G_R(\%)$	$W'(\%)$	SM(%)
Selection cuts	-2	-3	-2	7	-4 (± 1.2)
$m_{t\bar{t}} > 450 \text{ GeV}$	1	0	1	12	-2 (± 1.7)
$ y(t) + y(\bar{t}) > 2$	3	0	0	12	3 (± 3.2)

couplings to top quarks. Polarization measurements also are important for distinguishing the G_L model from the SM. The bias towards right-handed polarizations is an effect of selection cuts preferentially passing the harder leptons which arise from right-handed tops.

D. Top Spin Correlation

Finally, we present results on $t\bar{t}$ spin correlations

$$\mathcal{A}_{c_1 c_2}^\ell = \frac{N(c_1 c_2 > 0) - N(c_1 c_2 < 0)}{N(c_1 c_2 > 0) + N(c_1 c_2 < 0)} \quad (12)$$

where $c_1 = \cos \theta_{\ell_1, n}$ and $c_2 = \cos \theta_{\ell_2, n}$. As with the previous section, we present results using two polarization axes: the beam axis in Table X and the helicity axis in Table XI.

As one can see from the tables, $\mathcal{A}_{c_1 c_2}^\ell$ is not as sensitive to new physics effects as the observables explored in the previous subsections and thus will require more luminosity before yielding meaningful information. Nonetheless, as this observable probes independent information it should still be measured as it can help to further narrow down the set of explanatory models.

IV. CONCLUSIONS

As more analyses are completed, the anomalous top forward backward asymmetry observed at the Tevatron appears increasingly robust. The observed asymmetry has manifested itself across many channels, at different experiments, and appears to rise strongly with increasing $m_{t\bar{t}}$, suggestive of new physics. While a healthy dollop of skepticism is always warranted in interpreting this sort of anomaly, especially as it may be susceptible to subtle QCD effects, the measurement presents at the very least

one of the most compelling collider anomaly seen in recent years, and may be our first hint of the BSM effects we may hope to observe at the LHC.

Here we have considered various models built to explain the measured value of the top asymmetry. While all models yield an enhanced $t\bar{t}$ asymmetry, they yield distinct mixtures of left- and right-polarized tops. As the polarization of a top influences the kinematics of its decay products, especially the charged lepton, distributions built from the leptons in dileptonic and semileptonic $t\bar{t}$ events are powerful probes of the physics underlying the anomalous top forward backward asymmetry. Leptonic charge asymmetries are particularly attractive for these purposes. The potentially large central values of the lepton asymmetries make them sensitive probes of deviations from the SM, while the relationship between the lepton asymmetry and its parent $t\bar{t}$ asymmetry is a useful diagnostic of the chiral structure of the model. Published results for lepton charge asymmetries would be very useful for understanding the properties of any new physics contributing to the $t\bar{t}$ cross-section.

Turning to the LHC, we found that this machine, despite being a pp collider, has excellent prospects for shedding light on the top forward-backward asymmetry. We defined an asymmetry variable at the LHC where the forward direction is chosen event by event, exploiting the distinct kinematics of sea and valence quarks, and utilized it with a novel set of cuts designed to enhance the contributions of new physics. With our cuts and realistic reconstruction procedure, we are able to firmly establish the existence of a large BSM asymmetry within the first 5 fb^{-1} of data at the 7 TeV LHC. This result is based only on dileptonic tops, and the approach can easily be extended to the semileptonic channel, which promises a larger cross-section and better statistics. While a full detector-level simulation will be necessary to understand the ultimate LHC sensitivity, this approach seems promising and warrants further study.

We further observed that leptonic variables, namely lepton charge asymmetries, top polarizations, and $t\bar{t}$ spin correlations, are extremely valuable tools in distinguishing between the various new physics models which have been proposed to explain the anomalous AFB. Using only the nonresonant portion of the $t\bar{t}$ spectrum, we saw that a 7 TeV LHC is able to distinguish amongst various BSM models in as little as $\sim 5 \text{ fb}^{-1}$ of data.

ACKNOWLEDGMENTS

We would like to thank Claudio Campagnari, Qinghong Cao, Zhenyu Han, Dilani Kahawala, Matt Schwartz, Matt Strassler, Tim Tait, Paul Tipton, Yanjun Tu, Brock Tweedie, Itay Yavin, and Junjie Zhu for useful discussions, and particularly to thank Steve Giddings for collaborations in the early stage of this project. D.K., L.-T.W., and T.L. would like to thank Aspen Center for Physics for its hospitality. J.S. would like to thank

SLAC for its hospitality. The work of T.L. was supported in part by the Department of Energy under contract DE-FG02-91ER40618. D.K. is supported by a Simons postdoctoral fellowship and by an LHC-TI travel grant. J.S. was supported in part by DOE grant DE-FG02-92ER40704. L.-T.W. is supported by the NSF under grant PHY-0756966 and the DOE Early Career Award under grant DE-SC0003930.

Appendix A: Fully Leptonic Top Reconstruction

Fully leptonic di-top events yield two neutrinos, and so the top four-vector is not immediately accessible from the collider data. However, the eight unknowns comprising the two unmeasured neutrino four-vectors can be obtained if one requires:

- $p_\nu^2 = 0$
- $(p_\nu + p_l)^2 = m_W^2$
- $(p_\nu + p_l + p_b)^2 = m_t^2$
- $(p_{\nu_1} + p_{\nu_2})_{\{x,y\}} = (\not{E}_T)_{\{x,y\}}$

Each item above yields two conditions which must be satisfied, so that in total the eight conditions - enough to solve⁹ the system up to discrete ambiguities.

In practice, a reconstructed event can yield zero, two, or four neutrino solutions. If no neutrino solutions are found it could be because the top and/or W produced in the event was sufficiently off-shell to make solving the constraint equations (which take as input the particle pole masses) impossible, or because the jet four-momenta were smeared too far away from their true values. Events with two or four solutions can arise from the ambiguities in the solution to the constraint equations, and when there is an ambiguity in which b to assign to which lepton in computing m_t .

To choose the correct solution we employ a technique developed in [24] that assigns each neutrino solution a weight,

$$w = f(x)\bar{f}(x)p(E_l^*|m_t)p(E_l^*|m_t) \quad (\text{A1})$$

where E_l^* is the energy of the lepton in the reconstructed top quark rest frame,

$$p(E_l^*|m_t) = \frac{4E_l^*m_t(m_t^2 - m_b^2 - 2E_l^*m_t)}{(m_t^2 - m_b^2)^2 - m_W^2(m_t^2 + m_b^2) - 2m_w^4} \quad (\text{A2})$$

measures the likelihood that a top will decay into a lepton of rest frame energy E_l^* , and f (\bar{f}) are the relevant proton (anti-proton) PDFs¹⁰. In essence, this reconstruction

method picks the neutrino/top solution which, all things being equal, seemed most probable. For more details on the experimental implementation of this method we refer the reader to Ref. [26]. We also note that the method presented in Ref. [27] might provide a complementary procedure.

Appendix B: Models

To gauge the reach of the polarization and correlation techniques presented herein we have adopted a set of benchmark models. Here we will introduce these models and delineate their parameters.

As was mentioned in Sec. I, BSM models designed to explain the top forward-backward anomaly generally fall into two classes: s and t channel. The good agreement between observation and SM predictions for the top pair production cross-section makes it challenging to reproduce an asymmetry as large as the observed effect solely from BSM processes. If, instead, the asymmetry arises from the interference of BSM graphs with SM QCD pair production, a sizable asymmetry can be realized without comparably large positive-definite contributions to the top pair production cross-section. To obtain an asymmetric contribution from interference effects of the necessary size, the BSM graphs must have the same leading color and Lorentz structures as the $q\bar{q} \rightarrow t\bar{t}$ contribution to SM top pair production. From this condition, we determine that BSM particles exchanged in the s -channel must be spin 1 color octets, while particles exchanged in the t -channel can be either vectors or scalars, and can be in any color representation of QCD that appears in the product of two fundamentals or a fundamental and an anti-fundamental, namely 8, $\bar{3}$, 6, or 1.

For an s -channel particle to contribute to the asymmetry at tree level, its couplings to both initial and final states must be parity violating; otherwise any asymmetry will only be generated at loop level, as in QCD. We will call all such color vector octet particles *axigluons*, even though the term more properly refers only to such particles when they have a purely axial coupling. At the Tevatron, the axigluon is not produced on-shell, $m_A \gg \sqrt{s}$; in this regime, the leading contribution of the axigluon to the top asymmetry is determined by the mass of the axigluon and the product of axial couplings to the first and third generations, $A_{FB}^t \propto -g_A^1 g_A^3$. Note the sign: to yield a positive asymmetry, the couplings to first and third generations must have opposite signs. Once the mass and the product $g_A^1 g_A^3$ are fixed, the relative strength of the first and third generation axial couplings, as well as the vector-like couplings, can be varied, with only subleading effects on the asymmetry. Here, in order to highlight the importance of polarization, we choose three representative models which are all consistent with the Tevatron data, yet have their vector-like couplings adjusted to yield (1) a pure axial model; (2) a model which only couples to left-handed tops; and (3) a model

⁹ Many techniques are available to numerically solve the eight constraint conditions. For our work we use the methods presented in Ref. [23].

¹⁰ We use the CTEQ6.1 PDFs [25] for our analysis.

TABLE XII. The parameters used in our reference axigluon models. We fix the axigluon width to be 1.4 TeV

Model	M [TeV]	Γ [TeV]	g_1^A	g_1^V	g_3^A	g_3^V	g^A	g^V
G_A	2.0	1.40	-2.3	0.0	3.35	0.0	/	/
G_L	2.0	1.40	-2.3	0.0	3.35	3.35	/	/
G_R	2.0	1.40	-2.3	0.0	3.35	-3.35	/	/
W'	0.40	0.04	/	/	/	/	-0.90	0.90

which only couples to right-handed tops (see Table XII).

The axigluon width depends upon many quantities which are unrelated to the reproduction of the forward-backward asymmetry (such as the coupling to second generation quarks, and the coupling to the b); for simplicity we use a large constant width $\Gamma_G = 1.4$ TeV for all our reference models. As the LHC can access the axigluon pole mass (which is around 2 TeV) a substantial model dependence can arise if the events from this region are analyzed as part of our signal. We therefore take a conservative approach, explicitly removing this high invariant mass region from our analysis (see the discussion in Sec. III A).

In t -channel models, the asymmetry is generated by the kinematic structure of the amplitude, from the forward singularity of the t -channel propagator. In order to yield a large asymmetry without large corrections to the cross-section, the intermediate BSM state(s) must have dominantly flavor-off-diagonal couplings. Intermediate t channel states can be either scalar or vector; for a given additional contribution to the total $t\bar{t}$ cross-section, vectors give a greater enhancement to the asymmetry than do scalars. Intermediate vectors must couple to $\bar{q}q$ and therefore must be octets or singlets, while intermediate scalars can couple to either qq or $\bar{q}q$ and hence present more options. Large flavor-changing couplings are easier to accommodate if the coupling is only to right-handed quarks; t -channel models thus generically predict substantial top polarization. If the exchanged particle is self-conjugate, such as a Z' , then it will also mediate same-sign top production, $qq \rightarrow t\bar{t}$, the nondetection of which poses a stringent constraint.

As an example of this class of model, we adopt a flavor-off-diagonal W' which couples d_R to t_R ,

$$g_A = -0.9, \quad g_V = 0.9, \quad m_{W'} = 0.4 \text{ TeV}, \quad \Gamma = 0.04 \text{ TeV}; \quad (\text{B1})$$

this parameter set is one of the benchmark models of [10].

The $t\bar{t}$ cross-section and (Tevatron) A_{fb}^t which our benchmark reference models predict is presented in Table XIII along with a comparison to the SM. Results are shown at leading order, and without acceptance cuts; after incorporating realistic acceptance cuts, the apparently large cross-section predicted by the W' reference model is brought into better accord with measurements [10]. Note that the axigluon reference models, while consistent with cross-section measurements, somewhat underpredict the observed forward-backward asymmetry. We have chosen these points to be conservative:

TABLE XIII. The LO $t\bar{t}$ production cross sections at the Tevatron and the LHC for the benchmark models, along with the CM frame top asymmetry.

Model	$\sigma_{t\bar{t}}^{\text{Tevatron}}$ [pb]	$\sigma_{t\bar{t}}^{\text{LHC}}$ [pb]	A_{fb}^{Tevatron}
SM	5.6	89	0%
G_A	5.8	91	14%
G_L	6.1	95	13%
G_R	6.1	95	13%
W'	7.3	123	24%

models which realize a larger asymmetry are even easier to distinguish from the SM and from each other using the techniques presented here.

Appendix C: Tabulated Results for Leptonic Observables

Here we collect tabulated predictions for several leptonic observables for the SM and our reference models at both the Tevatron and the LHC. We show results for multiple angular variables, integrated to construct asymmetries.

For polarization variables we show the integrated asymmetry,

$$\mathcal{A}_{\cos\theta}^\ell = \frac{N(\cos\theta > 0) - N(\cos\theta < 0)}{N(\cos\theta > 0) + N(\cos\theta < 0)}. \quad (\text{C1})$$

For azimuthal correlations between leptons, we show

$$\mathcal{A}_{\Delta\phi}^\ell = \frac{N(\cos\Delta\phi_{\ell\ell} > 0) - N(\cos\Delta\phi_{\ell\ell} < 0)}{N(\cos\Delta\phi_{\ell\ell} > 0) + N(\cos\Delta\phi_{\ell\ell} < 0)}, \quad (\text{C2})$$

and for spin correlations we present the integrated variable

$$\mathcal{A}_{c_1c_2}^\ell = \frac{N(c_1c_2 > 0) - N(c_1c_2 < 0)}{N(c_1c_2 > 0) + N(c_1c_2 < 0)}. \quad (\text{C3})$$

For the Tevatron we collect here expected net polarizations in the beam (Tab. XIV) and off-diagonal bases (Tab. XV). Results are displayed at parton level, after acceptance cuts. To gauge the statistical significance of the asymmetries, note that in 5.3 fb^{-1} CDF observes 976.7 ± 91.2 signal events passing their semileptonic cuts [2]. As the statistical uncertainty on these asymmetry variables is to a good approximation simply given by $1/\sqrt{N}$, we then obtain a statistical error of 3% on asymmetry variables with current data. For dileptonic tops, in 5.1 fb^{-1} , CDF observes 237.1 ± 14.7 signal events passing cuts [5], for a statistical error of 6.5% on asymmetries. Going to the high mass region will reduce the number of events by a factor of 50%–60%. This procedure gives more conservative estimates of statistical significance than using the significance derived from the cross sections after our (parton level) selection cuts.

We also present parton-level results for dileptonic top variables at the 7 TeV LHC. Tab. XVII shows the resulting $t\bar{t}$ asymmetry and Tab. XVIII presents the related leptonic charge asymmetry. We further give the parton-level polarization and spin-correlation results: Tab. XIX shows the distribution of $\mathcal{A}_{\Delta\phi}^{ll}$, Tab. XX gives the top polarization using the beam-basis, while Tab. XXI presents this in the helicity basis, Tab. XXII shows the $t\bar{t}$ spin correlations in the beam basis, and finally Tab. XXIII shows these in the helicity basis.

TABLE XIV. Net polarization \mathcal{P}_b in the beam basis at the Tevatron.

	Semileptonic		Dileptonic	
	sel. cuts	$m_{t\bar{t}} > 450$ GeV	sel. cuts	$m_{t\bar{t}} > 450$ GeV
SM	-3 % (3 %)	-9 % (5 %)	-8 % (6.5%)	-14 % (10 %)
G_A	-5 %	-10 %	-5 %	-7 %
G_L	-2 %	-3 %	7 %	9 %
G_R	-6 %	-13 %	-17 %	-25 %
W'	-11 %	-19 %	-12 %	-21 %

TABLE XV. Net polarization $\mathcal{P}_{\text{off-d}}$ in the off-diagonal basis at the Tevatron.

	Semileptonic		Dileptonic	
	sel. cuts	$m_{t\bar{t}} > 450$ GeV	sel. cuts	$m_{t\bar{t}} > 450$ GeV
SM	-14 % (3 %)	-15 % (5 %)	-17 % (6.5 %)	-17 % (10 %)
G_A	-15 %	-15 %	-17 %	-17 %
G_L	-11 %	-7 %	-13 %	-10 %
G_R	-17 %	-19 %	-20 %	-23 %
W'	-24 %	-30 %	-24 %	-30 %

TABLE XVI. The cross section, in pb, for leptonically decaying di-top events at a 7 TeV LHC, and in parenthesis the 1σ uncertainties on an asymmetry measurement centered about zero assuming 5 fb^{-1} of data (i.e. $1/\sqrt{N}$).

	G_A	G_L	G_R	W'	SM
Selection cuts	2.1	2.2	2.2	3.3	2.1($\pm 1.0\%$)
$m_{t\bar{t}} > 450$ GeV	1.1	1.2	1.2	2.2	1.1($\pm 1.3\%$)
$ y(t) + y(\bar{t}) > 2$	0.3	0.3	0.3	0.5	0.2($\pm 3.2\%$)

TABLE XVII. The top forward-backward asymmetry $\mathcal{A}^{t\bar{t}}$ at a 7 TeV LHC

	$G_A(\%)$	$G_L(\%)$	$G_R(\%)$	$W'(\%)$	SM($\%$)
Selection cuts	2	2	3	15	0
$m_{t\bar{t}} > 450$ GeV	4	3	5	21	1
$ y(t) + y(\bar{t}) > 2$	8	7	11	38	2

TABLE XVIII. The forward-central lepton asymmetry \mathcal{A}_{FC}^ℓ at a 7 TeV LHC

	$G_A(\%)$	$G_L(\%)$	$G_R(\%)$	$W'(\%)$	SM($\%$)
Selection cuts	2	0	5	14	0
$m_{t\bar{t}} > 450$ GeV	3	1	6	20	0
$ y(t) + y(\bar{t}) > 2$	6	2	14	37	0

TABLE XIX. The azimuthal angle asymmetry $\mathcal{A}_{\Delta\phi}^{ll}$ at a 7 TeV LHC

	$G_A(\%)$	$G_L(\%)$	$G_R(\%)$	$W'(\%)$	SM($\%$)
Selection cuts	-23	-24	-26	-40	-21
$m_{t\bar{t}} > 450$ GeV	-43	-44	-46	-58	-41
$ y(t) + y(\bar{t}) > 2$	-40	-45	-48	-54	-41

TABLE XX. Net polarization \mathcal{P}_b in the beam basis at a 7 TeV LHC

	$G_A(\%)$	$G_L(\%)$	$G_R(\%)$	$W'(\%)$	SM($\%$)
Selection cuts	0	-2	3	6	0
$m_{t\bar{t}} > 450$ GeV	0	-2	3	9	-1
$ y(t) + y(\bar{t}) > 2$	1	-8	9	13	-1

TABLE XXI. Net polarization \mathcal{P}_h in the helicity basis at a 7 TeV LHC

	$G_A(\%)$	$G_L(\%)$	$G_R(\%)$	$W'(\%)$	SM($\%$)
Selection cuts	5	3	9	21	5
$m_{t\bar{t}} > 450$ GeV	6	2	11	28	6
$ y(t) + y(\bar{t}) > 2$	8	4	11	25	5

TABLE XXII. Spin correlation asymmetry $\mathcal{A}_{c_1c_2}^\ell$ in the beam basis at a 7 TeV LHC

	$G_A(\%)$	$G_L(\%)$	$G_R(\%)$	$W'(\%)$	SM($\%$)
Selection cuts	-2	-2	-3	-6	-3
$m_{t\bar{t}} > 450$ GeV	-5	-5	-5	-9	-5
$ y(t) + y(\bar{t}) > 2$	-7	-8	-10	-10	-8

TABLE XXIII. Spin correlation asymmetry $\mathcal{A}_{c_1c_2}^\ell$ in the helicity basis at a 7 TeV LHC

	$G_A(\%)$	$G_L(\%)$	$G_R(\%)$	$W'(\%)$	SM($\%$)
Selection cuts	-5	-4	-4	4	-6
$m_{t\bar{t}} > 450$ GeV	-2	-1	0	10	-3
$ y(t) + y(\bar{t}) > 2$	0	1	3	10	0

- [1] T. Aaltonen *et al.* (CDF Collaboration), *Phys.Rev.Lett.*, **101**, 202001 (2008), arXiv:0806.2472 [hep-ex]; V. Abazov *et al.* (D0 Collaboration), *ibid.*, **100**, 142002 (2008), arXiv:0712.0851 [hep-ex].
- [2] T. Aaltonen *et al.* (CDF Collaboration), *Phys.Rev.D* (2011), arXiv:1101.0034 [hep-ex].
- [3] M. Bowen, S. Ellis, and D. Rainwater, *Phys.Rev.*, **D73**, 014008 (2006), arXiv:hep-ph/0509267 [hep-ph].
- [4] J. H. Kuhn and G. Rodrigo, *Phys.Rev.*, **D59**, 054017 (1999), arXiv:hep-ph/9807420 [hep-ph]; O. Antunano, J. H. Kuhn, and G. Rodrigo, *ibid.*, **D77**, 014003 (2008), arXiv:0709.1652 [hep-ph]; L. G. Almeida, G. F. Sterman, and W. Vogelsang, *ibid.*, **D78**, 014008 (2008), arXiv:0805.1885 [hep-ph].
- [5] CDF note 103098, <http://www-cdf.fnal.gov/physics/new/top/2011/DilAfb/>.
- [6] A. Djouadi, G. Moreau, F. Richard, and R. K. Singh, *Phys.Rev.*, **D82**, 071702 (2010), arXiv:0906.0604 [hep-ph]; M. Martynov and A. Smirnov, *Mod.Phys.Lett.*, **A24**, 1897 (2009), arXiv:0906.4525 [hep-ph]; P. Ferrario and G. Rodrigo, *Phys.Rev.*, **D80**, 051701 (2009), arXiv:0906.5541 [hep-ph]; S. Jung, H. Murayama, A. Pierce, and J. D. Wells, *ibid.*, **D81**, 015004 (2010), arXiv:0907.4112 [hep-ph]; K. Cheung, W.-Y. Keung, and T.-C. Yuan, *Phys.Lett.*, **B682**, 287 (2009), arXiv:0908.2589 [hep-ph]; J. Frampton, Paul H. and K. Wang, *ibid.*, **B683**, 294 (2010), arXiv:0911.2955 [hep-ph]; J. Shu, T. M. Tait, and K. Wang, *Phys.Rev.*, **D81**, 034012 (2010), arXiv:0911.3237 [hep-ph]; A. Arhrib, R. Benbrik, and C.-H. Chen, *ibid.*, **D82**, 034034 (2010), arXiv:0911.4875 [hep-ph]; I. Dorsner, S. Fajfer, J. F. Kamenik, and N. Kosnik, *ibid.*, **D81**, 055009 (2010), arXiv:0912.0972 [hep-ph]; V. Barger, W.-Y. Keung, and C.-T. Yu, *ibid.*, **D81**, 113009 (2010), arXiv:1002.1048 [hep-ph]; J. Cao, Z. Heng, L. Wu, and J. M. Yang, *ibid.*, **D81**, 014016 (2010), arXiv:0912.1447 [hep-ph]; Q.-H. Cao, D. McKeen, J. L. Rosner, G. Shaughnessy, and C. E. Wagner, *ibid.*, **D81**, 114004 (2010), arXiv:1003.3461 [hep-ph]; B. Xiao, Y.-k. Wang, and S.-h. Zhu, *ibid.*, **D82**, 034026 (2010), arXiv:1006.2510 [hep-ph]; M. Martynov and A. Smirnov, *Mod.Phys.Lett.* (2010), arXiv:1006.4246 [hep-ph]; R. Chivukula, E. H. Simmons, and C.-P. Yuan, *Phys.Rev.*, **D82**, 094009 (2010), arXiv:1007.0260 [hep-ph]; G. Rodrigo and P. Ferrario, (2010), arXiv:1007.4328 [hep-ph]; M. Bauer, F. Goertz, U. Haisch, T. Pfoh, and S. Westhoff, *JHEP*, **1011**, 039 (2010), arXiv:1008.0742 [hep-ph]; C. Zhang and S. Willenbrock, *Phys.Rev.*, **D83**, 034006 (2011), arXiv:1008.3869 [hep-ph]; C.-H. Chen, G. Cvetič, and C. Kim, *Phys.Lett.*, **B694**, 393 (2011), arXiv:1009.4165 [hep-ph]; B. Xiao, Y.-k. Wang, and S.-h. Zhu, (2010), arXiv:1011.0152 [hep-ph]; E. Alvarez, L. Da Rold, and A. Szykman, (2010), arXiv:1011.6557 [hep-ph]; G. Burdman, L. de Lima, and R. D. Matheus, *Phys.Rev.*, **D83**, 035012 (2011), arXiv:1011.6380 [hep-ph]; K. Cheung and T.-C. Yuan, (2011), arXiv:1101.1445 [hep-ph]; Y. Bai, J. L. Hewett, J. Kaplan, and T. G. Rizzo, *JHEP*, **1103**, 003 (2011), arXiv:1101.5203 [hep-ph]; J. Shelton and K. M. Zurek, (2011), arXiv:1101.5392 [hep-ph]; V. Barger, W.-Y. Keung, and C.-T. Yu, (2011), arXiv:1102.0279 [hep-ph]; K. Blum, C. Delaunay, O. Gedalia, Y. Hochberg, S. J. Lee, *et al.*, (2011), arXiv:1102.3133 [hep-ph]; B. Grinstein, A. L. Kagan, M. Trott, and J. Zupan, (2011), arXiv:1102.3374 [hep-ph]; K. M. Patel and P. Sharma, (2011), arXiv:1102.4736 [hep-ph]; A. R. Zerwekh, (2011), arXiv:1103.0956 [hep-ph]; C. Delaunay, O. Gedalia, Y. Hochberg, G. Perez, and Y. Soreq, (2011), arXiv:1103.2297 [hep-ph]; Z. Ligeti, M. Schmaltz, and G. M. Tavares, (2011), arXiv:1103.2757 [hep-ph]; A. L. Kagan, J. F. Kamenik, G. Perez, and S. Stone, (2011), arXiv:1103.3747 [hep-ph]; S. Jung, A. Pierce, and J. D. Wells, (2011), arXiv:1103.4835 [hep-ph]; M. R. Buckley, D. Hooper, J. Kopp, and E. Neil, (2011), arXiv:1103.6035 [hep-ph]; J. Shu, K. Wang, and G. Zhu, (2011), arXiv:1104.0083 [hep-ph]; A. Rajaraman, Z. Surujon, and T. M. Tait, (2011), arXiv:1104.0947 [hep-ph]; J. Aguilar-Saavedra and M. Perez-Victoria, (2011), arXiv:1104.1385 [hep-ph]; C.-H. Chen, S. S. Law, and R.-H. Li, (2011), arXiv:1104.1497 [hep-ph]; A. E. Nelson, T. Okui, and T. S. Roy, (2011), arXiv:1104.2030 [hep-ph]; X.-P. Wang, Y.-K. Wang, B. Xiao, J. Xu, and S.-h. Zhu, (2011), arXiv:1104.1917 [hep-ph]; L. A. Anchordoqui, H. Goldberg, X. Huang, D. Lust, and T. R. Taylor, (2011), arXiv:1104.2302 [hep-ph]; S. Jung, A. Pierce, and J. D. Wells, (2011), arXiv:1104.3139 [hep-ph]; G. Zhu, (2011), arXiv:1104.3227 [hep-ph]; P. J. Fox, J. Liu, D. Tucker-Smith, and N. Weiner, (2011), arXiv:1104.4127 [hep-ph]; D.-W. Jung, P. Ko, and J. S. Lee, (2011), arXiv:1104.4443 [hep-ph]; K. Babu, M. Frank, and S. K. Rai, (2011), arXiv:1104.4782 [hep-ph]; Q.-H. Cao, M. Carena, S. Gori, A. Menon, P. Schwaller, *et al.*, (2011), arXiv:1104.4776 [hep-ph]; A. Djouadi, G. Moreau, and F. Richard, *Phys.Lett.*, **B701**, 458 (2011), * Temporary entry *, arXiv:1105.3158 [hep-ph].
- [7] C. Degrande, J.-M. Gerard, C. Grojean, F. Maltoni, and G. Servant, (2010), arXiv:1010.6304 [hep-ph]; J. Aguilar-Saavedra and M. Perez-Victoria, (2011), arXiv:1103.2765 [hep-ph].
- [8] Y.-k. Wang, B. Xiao, and S.-h. Zhu, *Phys.Rev.*, **D82**, 094011 (2010), arXiv:1008.2685 [hep-ph]; B. Xiao, Y.-K. Wang, Z.-Q. Zhou, and S.-h. Zhu, (2011), arXiv:1101.2507 [hep-ph]; J. Cao, L. Wang, L. Wu, and J. M. Yang, (2011), arXiv:1101.4456 [hep-ph]; B. Bhattacherjee, S. S. Biswal, and D. Ghosh, (2011), arXiv:1102.0545 [hep-ph].
- [9] N. Craig, C. Kilic, and M. J. Strassler, (2011), arXiv:1103.2127 [hep-ph].
- [10] M. I. Gresham, I.-W. Kim, and K. M. Zurek, (2011), arXiv:1103.3501 [hep-ph].
- [11] J. L. Hewett, J. Shelton, M. Spannowsky, T. M. Tait, and M. Takeuchi, (2011), arXiv:1103.4618 [hep-ph].
- [12] D.-W. Jung, P. Ko, J. S. Lee, and S.-h. Nam, *Phys.Lett.*, **B691**, 238 (2010), arXiv:0912.1105 [hep-ph].
- [13] V. D. Barger, J. Ohnemus, and R. Phillips, *Int.J.Mod.Phys.*, **A4**, 617 (1989); G. L. Kane, G. Ladinisky, and C. Yuan, *Phys.Rev.*, **D45**, 124 (1992); C. R. Schmidt and M. E. Peskin, *Phys.Rev.Lett.*, **69**, 410 (1992); A. Brandenburg and J. Ma, *Phys.Lett.*, **B298**, 211 (1993); M. Jezabek and J. H. Kuhn, *ibid.*, **B329**, 317 (1994), arXiv:hep-ph/9403366 [hep-ph]; G. Mahlon

- and S. J. Parke, Phys.Rev., **D53**, 4886 (1996), arXiv:hep-ph/9512264 [hep-ph].
- [14] K. Agashe, A. Belyaev, T. Krupovnickas, G. Perez, and J. Virzi, Phys.Rev., **D77**, 015003 (2008), arXiv:hep-ph/0612015 [hep-ph]; B. Lillie, L. Randall, and L.-T. Wang, JHEP, **0709**, 074 (2007), arXiv:hep-ph/0701166 [hep-ph]; D. Krohn, J. Shelton, and L.-T. Wang, *ibid.*, **1007**, 041 (2010), arXiv:0909.3855 [hep-ph]; M. Baumgart and B. Tweedie, (2011), arXiv:1104.2043 [hep-ph]; E. L. Berger, Q.-H. Cao, C.-R. Chen, and H. Zhang, Phys.Rev., **D83**, 114026 (2011), arXiv:1103.3274 [hep-ph]; A. Djouadi, G. Moreau, and R. K. Singh, Nucl.Phys., **B797**, 1 (2008), arXiv:0706.4191 [hep-ph].
- [15] R. M. Godbole, K. Rao, S. D. Rindani, and R. K. Singh, JHEP, **1011**, 144 (2010), arXiv:1010.1458 [hep-ph]; D.-W. Jung, P. Ko, and J. S. Lee, (2010), arXiv:1011.5976 [hep-ph]; D. Choudhury, R. M. Godbole, S. D. Rindani, and P. Saha, (2010), arXiv:1012.4750 [hep-ph]; J. Cao, L. Wu, and J. M. Yang, (2010), arXiv:1011.5564 [hep-ph]; K. Melnikov and M. Schulze, *ibid.*, **0908**, 049 (2009), arXiv:0907.3090 [hep-ph]; W. Bernreuther and Z.-G. Si, Nucl.Phys., **B837**, 90 (2010), arXiv:1003.3926 [hep-ph].
- [16] A. Brandenburg, Z. Si, and P. Uwer, Phys.Lett., **B539**, 235 (2002), arXiv:hep-ph/0205023 [hep-ph]; J. Shelton, Phys.Rev., **D79**, 014032 (2009), arXiv:0811.0569 [hep-ph].
- [17] S. J. Parke and Y. Shadmi, Phys.Lett., **B387**, 199 (1996), arXiv:hep-ph/9606419 [hep-ph].
- [18] J. Alwall, P. Demin, S. de Visscher, R. Frederix, M. Herquet, *et al.*, JHEP, **0709**, 028 (2007), arXiv:0706.2334 [hep-ph].
- [19] T. Sjostrand, S. Mrenna, and P. Z. Skands, JHEP, **0605**, 026 (2006), arXiv:hep-ph/0603175 [hep-ph]; Comput.Phys.Commun., **178**, 852 (2008), arXiv:0710.3820 [hep-ph].
- [20] M. Cacciari, G. P. Salam, and G. Soyez, JHEP, **04**, 063 (2008), arXiv:0802.1189 [hep-ph].
- [21] M. Cacciari, G. Salam, and G. Soyez, “FastJet,” [Http://fastjet.fr/](http://fastjet.fr/); M. Cacciari and G. P. Salam, Phys. Lett., **B641**, 57 (2006), arXiv:hep-ph/0512210.
- [22] V. Khachatryan *et al.* (CMS Collaboration), Phys.Lett., **B695**, 424 (2011), arXiv:1010.5994 [hep-ex].
- [23] L. Sonnenschein, Phys.Rev., **D73**, 054015 (2006), arXiv:hep-ph/0603011 [hep-ph].
- [24] R. Dalitz and G. R. Goldstein, Phys.Rev., **D45**, 1531 (1992).
- [25] D. Stump, J. Huston, J. Pumplin, W.-K. Tung, H. Lai, *et al.*, JHEP, **0310**, 046 (2003), arXiv:hep-ph/0303013 [hep-ph].
- [26] D. D. Boline, (2010), ph.D. Thesis (Advisor: Ulrich Heintz).
- [27] Y. Bai and Z. Han, JHEP, **0904**, 056 (2009), arXiv:0809.4487 [hep-ph].